PCCP

Accepted Manuscript

ROYAL SOCIETY OF CHEMISTRY

www.rsc.org/pccp

Graphical abstract:

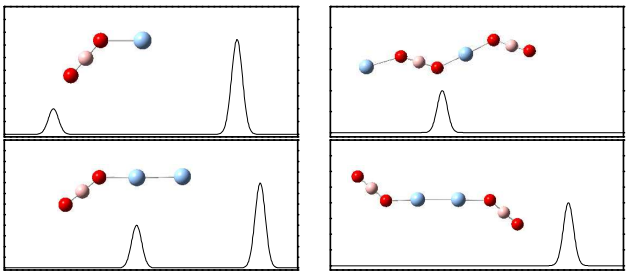

We identified hyperhalogens in $Ag_n(BO_2)_m$ (n=1-3, m=1-2) clusters by using anion photoelectron spectroscopy and density functional calculations.

Identification of Hyperhalogens in $Ag_n(BO_2)_m$ (n=1-3, m=1-2) Clusters: Anion Photoelectron Spectroscopy and Density Functional Calculations

Xiang-Yu Kong,[1] Hong-Guang Xu,[1] Pratik Koirala,[2] Wei-Jun Zheng,[*, 1] Anil K. Kandalam,[*, 3] and Puru Jena [4]

[1]*Beijing National Laboratory for Molecular Sciences, State Key Laboratory of Molecular Reaction Dynamics, Institute of Chemistry, Chinese Academy of Sciences, Beijing 100190, China*

[2]*Department of Materials Science and Engineering, Northwestern University, Evanston, IL 60208, USA*

[3]*Department of Physics, West Chester University, West Chester, PA 19383, USA*

[4]*Department of Physics, Virginia Commonwealth University, Richmond, VA 23284, USA*

* Corresponding author. E-mail: zhengwj@iccas.ac.cn, akandalam@wcupa.edu

Abstract

The electronic and structural properties of neutral and anionic $Ag_n(BO_2)_m$ (n=1-3, m=1-2) clusters are investigated by using mass-selected anion photoelectron spectroscopy and density functional theory calculations. Agreement between the measured and calculated vertical detachment energies (VDEs) allows us to validate the equilibrium geometries of $[Ag_n(BO_2)_m]^-$ clusters obtained from theory. The ground state structures of anionic $Ag_2(BO_2)$ and $Ag_n(BO_2)_2$ (n=1-3) clusters are found to be very different from those of their neutral counterparts. The structures of anionic clusters are chain-like while those of the neutral clusters are closed-rings. The presence of multiple isomers for $[Ag_2(BO_2)_2]^-$ and $[Ag_3(BO_2)_2]^-$ in the cluster beam is also been confirmed. Several of these clusters are found to be *hyperhalogens*.

I. INTRODUCTION

High electron affinity (EA) species are strong oxidizing agents, capable of oxidizing inert elements to form novel compounds with potential applications for new materials.[1,2] Among all the elements in the periodic table, the ones having the highest EAs are halogens, among which chlorine has the highest value (3.62 eV).[3] The species in the form of MX_{k+1} or $MO_{(k+1)/2}$ with EAs higher than that of chlorine were termed "superhalogens" by Gutsev and Boldyrev,[4] where M is a transition metal or main group atom, X is a halogen atom, and k is the maximal formal valence of the M atom. The halogens are important building blocks of superhalogens. In the last decades, many theoretical and experimental studies[5-27] have been conducted to investigate the unusual properties of a series of superhalogen molecules formed by metal atoms and halogen atoms.

Similar to the halogens, superhalogens themselves can also serve as building blocks in forming new species with even larger EAs. In a joint experimental and theoretical study, unusually stable $Au_n(BO_2)$ clusters (n = 1 – 5) exhibiting superhalogen properties were reported earlier by two of the current authors.[27] Following this study, the same authors, along with their experimental collaborators, reported[28] a new class of highly electronegative species, called hyperhalogens. These hyperhalogens can be synthesized by replacing the peripheral halogen atoms in a traditional superhalogen, with superhalogen units. These resulting hyperhalogens exhibit EA values that are even higher than the EAs of their superhalogen building-blocks. A series of hyperhalogen species have been studied experimentally and theoretically in a short period of time, such as $Au(BO_2)_2$, $Cu(BO_2)_2$,[28, 29] $Na(BO_2)_2$, $Al(BO_2)_4$,[30, 31] and $Na(BF_4)_2$,[32] and even extending to "magnetic hyperhalogens" such as $Mn(BO_2)_n$ and $Fe(BO_2)_n$ (n=3,4) clusters.[33] Recently, $Ag(BO_2)_2$ hyperhalogen and its corresponding anion, $[Ag(BO_2)_2]^-$ cluster were investigated by photoelectron spectroscopy and high-level ab initio calculations that included spin-orbit coupling (SOC).[34] In the current work, we extend the study to neutral and anionic $Ag_n(BO_2)_m$ (n=1-3, m=1-2) clusters using photoelectron spectroscopy and density functional calculations in order to investigate interactions between Ag and BO_2 and to explore the

possibility of forming new high electronegative species. In the following we briefly describe our experimental and theoretical methods. The results are presented and discussed in Section III. A summary of our conclusions is given in Section IV.

II. EXPERIMENTAL AND THEORETICAL METHODS

Experimental

The negative ion photoelectron spectra of $[Ag_n(BO_2)_m]^-$ (n=1-3, m=1-2) clusters are measured on a home-built apparatus consisting of a time-of-flight mass spectrometer (TOF-MS) and a magnetic-bottle photoelectron spectrometer, which has been described elsewhere.[35] Briefly, the $[Ag_n(BO_2)_m]^-$ (n=1-3, m=1-2) clusters are produced in a laser vaporization source by ablating a rotating translating disk target (13 mm diameter, Ag/B/Ag_2O mole ratio 5:1:1) with the second harmonic (532nm) light pulses of a Nd:YAG laser (Continuum Surelite II-10). Simultaneously, high purity helium with ~4 atm backing pressure is injected into the source by a pulsed valve (General Valve Series 9) to cool the formed clusters. The cluster anions are mass-analyzed by the time-of-flight mass spectrometer. The size-selected cluster anions of interest are decelerated before entering the photodetachment region. The $[Ag_n(BO_2)_m]^-$ (n=1-3, m=1-2) clusters were photodetached with the 193 nm photons from an ArF excimer laser (Model PSX-100, MPB Communications Inc.). The photoelectrons are energy-analyzed by the magnetic-bottle photoelectron spectrometer. The photoelectron spectra are calibrated by the spectrum of Ag^- taken at similar conditions. The energy resolution of the photoelectron spectrometer is ~40 meV at the electron kinetic energy of 1 eV.

Theoretical

The DFT calculations of neutral and negatively charged $Ag_n(BO_2)_m$ (n=1-3, m=1-2) clusters are carried out by employing the ωB97XD[36] functional implemented in the Gaussian 09 program package.[37] The 6-311++g(3df) basis set for B and O atoms, and Lanl2dz basis set with the effective

core potentials (ECPs) for Ag atoms are used in these calculations. All the geometry optimizations are performed without any symmetry constraint. The harmonic vibrational frequencies are calculated to confirm that the optimized structures correspond to real local minima. The calculated energies are corrected by the zero-point vibrational energies except for the vertical detachment energies (VDEs). The VDEs are calculated as the energy differences between the anion and neutral clusters at the anion ground state geometries. The adiabatic detachment energies (ADEs) are obtained as the energy differences between the anions and the optimized neutral clusters using the anion structures as the initial structures. The natural population analysis (NPA) are also conducted for the $[Ag_n(BO_2)_m]^-$ clusters.

In order to select the suitable theoretical method for the $Ag_n(BO_2)_m$ (n=1-3, m=1-2) clusters, we have tested B3LYP,[38, 39] M06-2X,[40] and ωB97XD functionals by calculating the VDEs of $[M(BO_2)_2]^-$ (M=Cu, Ag, and Au) and comparing them with the experimental measurements. Figure 1 shows the comparison between the calculated VDEs of $[M(BO_2)_2]^-$ with the experimental values.[28, 29, 34] It is found that the B3LYP functional overestimates the VDE of $[Cu(BO_2)_2]^-$ by only 0.06 eV but underestimates those of $[Ag(BO_2)_2]^-$ and $[Au(BO_2)_2]^-$ significantly by 0.67 and 0.29 eV respectively. The M06-2X functional, on the other hand, overestimates the VDE of $[Ag(BO_2)_2]^-$ by only 0.1 eV but overestimates those of $[Cu(BO_2)_2]^-$ and $[Au(BO_2)_2]^-$ by 0.61 and 0.42 eV, respectively. The ωB97XD functional underestimates the VDE of $[Ag(BO_2)_2]^-$ by only 0.1 eV and overestimates those of $[Cu(BO_2)_2]^-$ and $[Au(BO_2)_2]^-$ by 0.33 and 0.13 eV respectively. Overall, the ωB97XD functional gives more consistent results for all the three species. The results of ωB97XD are also in good agreement with the high level CCSD(T)/CBS calculations including the spin-orbit coupling.[34] Therefore, we used the ωB97XD functional in this work.

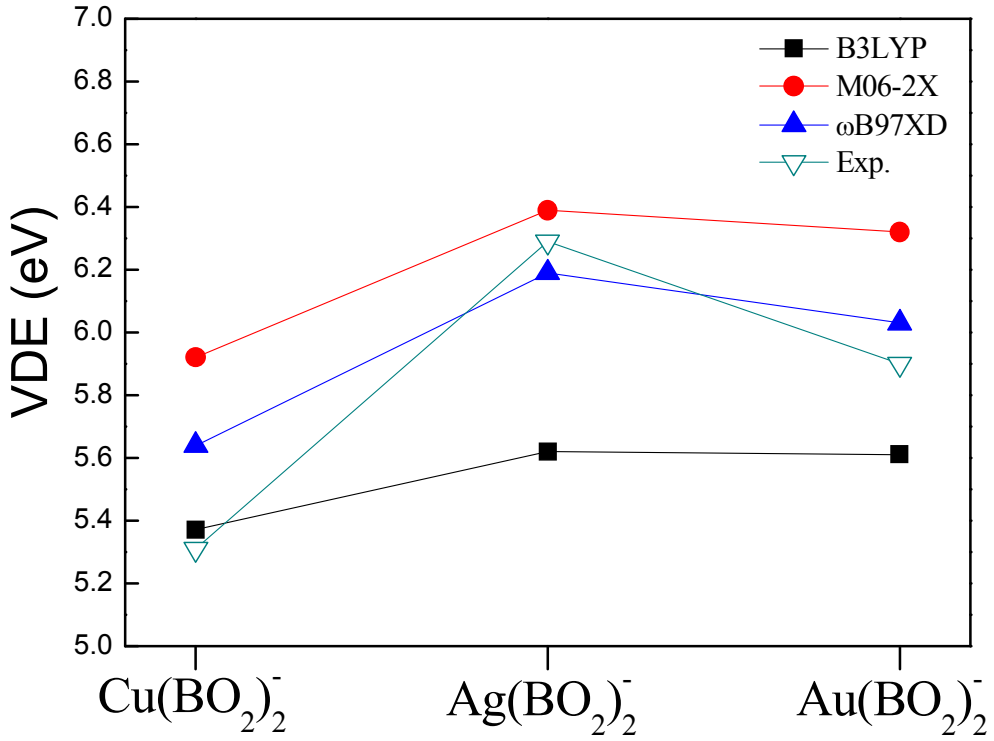

Figure 1. Experimental and calculated VDEs of $M(BO_2)_2^-$ (M=Cu, Ag, Au) using different theoretical methods. The experimental VDEs of $Cu(BO_2)_2^-$ and $Au(BO_2)_2^-$ are from [Ref 28] and [Ref 27], respectively.

III. RESULTS AND DISCUSSION

Experimental Results

The photoelectron spectra of $[Ag_n(BO_2)_m]^-$ (n=1-3, m=1-2) clusters recorded with 193 nm photons are presented in Figure 2. The spectrum of $[Ag(BO_2)_2]^-$ has been reported in our previous paper[34] and is shown here for comparison. The vertical detachment energies (VDEs) and the adiabatic detachment energies (ADEs) of $[Ag_n(BO_2)_m]^-$ (n=1-3, m=1-2) extracted from their photoelectron spectra are list in Table I. The VDEs are estimated from the maxima point of the first peaks. The ADEs are determined by drawing a straight line along the leading edge of the first peak to the baseline of the spectrum and adding the instrumental resolution to the electron binding energy

(EBE) value at the crossing point.

Table I. Experimental VDEs and ADEs estimated from the photoelectron spectra of $Ag_n(BO_2)_m^-$ (n=1-3, m=1-2)

Cluster	VDE (eV)	ADE (eV)
$AgBO_2^-$	2.39	2.10
$Ag_2BO_2^-$	3.77	3.59
$Ag(BO_2)_2^-$	6.28	6.20
$Ag_2(BO_2)_2^-$	3.32	2.87
$Ag_3(BO_2)_2^-$	4.17	3.79

As shown in Figure 2, the photoelectron spectrum of $[Ag(BO_2)]^-$ cluster reveals two peaks centered at 2.39 and 5.44 eV, respectively. In the spectrum of $[Ag_2(BO_2)]^-$ cluster, there are two clear features centered at 3.77 and 5.84 eV, respectively. As the number of Ag atoms increases, the first peak of $[Ag_n(BO_2)]^-$ (n=1-2) moves to higher electron binding energy region. The second peak also moves a little towards the high electron binding energy zone. In the spectrum of $[Ag_2(BO_2)_2]^-$ cluster, we can see that there is one feature centered at 3.32 eV and a broad feature in the range of 5.20 to 6.00 eV. The photoelectron spectrum of $[Ag_3(BO_2)_2]^-$ cluster shows two features centered at 4.17 and 4.98 eV, and an unresolved feature from 5.70 eV to higher EBE region.

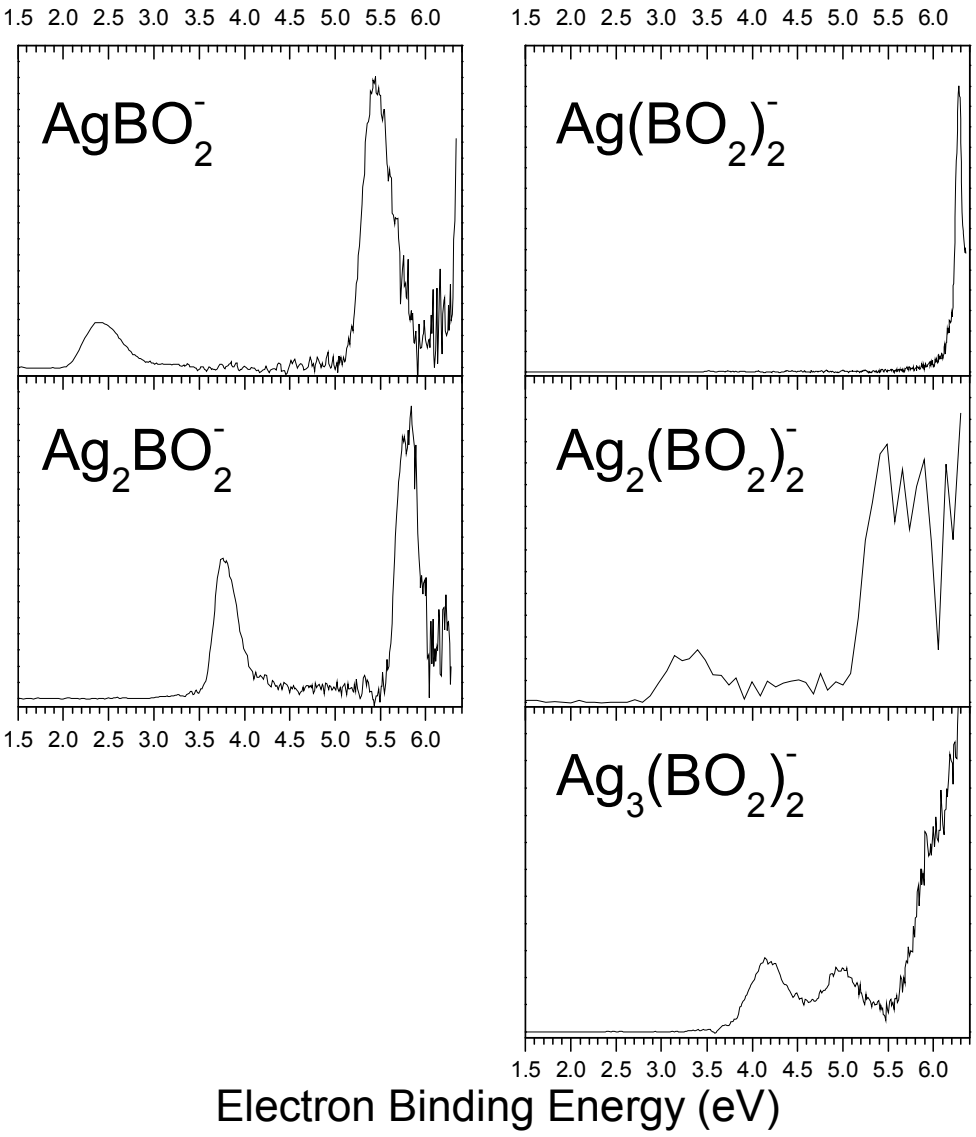

Figure 2. Photoelectron spectra of $Ag_n(BO_2)_m^-$ (n=1-3, m=1-2) clusters recorded with 193 nm photons.

Theoretical Results

The theoretical VDEs and ADEs of the low-lying isomers of $[Ag_n(BO_2)_m]^-$ (n=1-3, m=1-2) clusters are listed in Table II along with the experimental VDEs and ADEs for comparison. We have also simulated the photoelectron spectra of different isomers based on theoretically generalized Koopmans' theorem (GKT)[41, 42] and compared the simulated spectra with the experimental results in Figure 6. For convenience, we call the simulated spectra as density of states (DOS) spectra.[42] In the

simulated DOS spectra, the peak of each transition corresponds to the removal of an electron from a specific molecular orbital of the cluster anion. The process of the simulations have been described in details elsewhere.[43] Briefly, we first set the peak associated with the HOMO to the position of calculated VDE of each isomer, and shifted the peaks of the deeper orbitals according to their relative energies compared to the highest-occupied molecular orbital (HOMO).

Table II. Calculated VDEs and experimental VEDs for $Ag_n(BO_2)_m^-$ (n=1-3; m=1-2) clusters. The 6-311++G(3df) basis set for B and O atoms, and Lanl2dz basis set for Ag were used.

	Isomer	ΔE (eV)	VDE (eV)		ADE (eV)	
			ωB97XD	Exp.	ωB97XD	Exp.
$AgBO_2^-$	I	0	2.32	2.39	2.13	2.10
$Ag_2BO_2^-$	I	0	3.71	3.77	3.60	3.59
$Ag(BO_2)_2^-$	I	0	6.25	6.28	6.14	6.20
$Ag_2(BO_2)_2^-$	I	0	3.37	3.32	3.06	2.87
	II	0.02	5.49	5.64	3.04	
$Ag_3(BO_2)_2^-$	I	0	4.01	4.17	3.19	3.79
	II	0.09	4.91	4.98	3.09	
	III	0.13	5.89	5.91	3.06	

* Here, the calculated ADEs of $Ag_2(BO_2)_2^-$ and $Ag_3(BO_2)_2^-$ are very different from their calculated VDEs and the experimental ADEs because there are the significant structural changes between the anions and neutrals.

A. Ag_nBO_2 (n = 1, 2) clusters:

The ground state geometries of anionic and neutral $Ag(BO_2)$ clusters are identical to each other [Fig. 3(a) and Fig. 3(b), respectively] with the Ag atom binding to the oxygen atom of the BO_2 superhalogen moiety. The bond length between Ag and the O atoms of BO_2 increased from 2.08 Å to 2.28 Å as an extra electron was added to the $Ag(BO_2)$ cluster. As expected, the geometries of both neutral and anionic $Ag(BO_2)$ clusters are similar to that of $Au(BO_2)$ and $Cu(BO_2)$ clusters reported earlier.[27, 29] The calculated VDE and ADE values of $[Ag(BO_2)]^-$ cluster are 2.32 and 2.13 eV, respectively, which agree well with the experimental values (2.39 and 2.10 eV). In Figure 6, we can

also see that the simulated DOS spectrum of $[Ag(BO_2)]^-$ agrees well with the experimental photoelectron spectrum of $[Ag(BO_2)]^-$ cluster. Note that the VDE/ADE values of anionic $Ag(BO_2)$ cluster lie between the previously reported VDE/ADE values of anionic $Cu(BO_2)$ [2.17/2.04 eV][29] and anionic $Au(BO_2)$ clusters [3.34/3.06 eV].[27] Since, the lowest energy structures of neutral and anionic clusters are similar, the measured ADE value of $[Ag(BO_2)]^-$ cluster is equal to the electron affinity (EA) of neutral $Ag(BO_2)$ cluster.

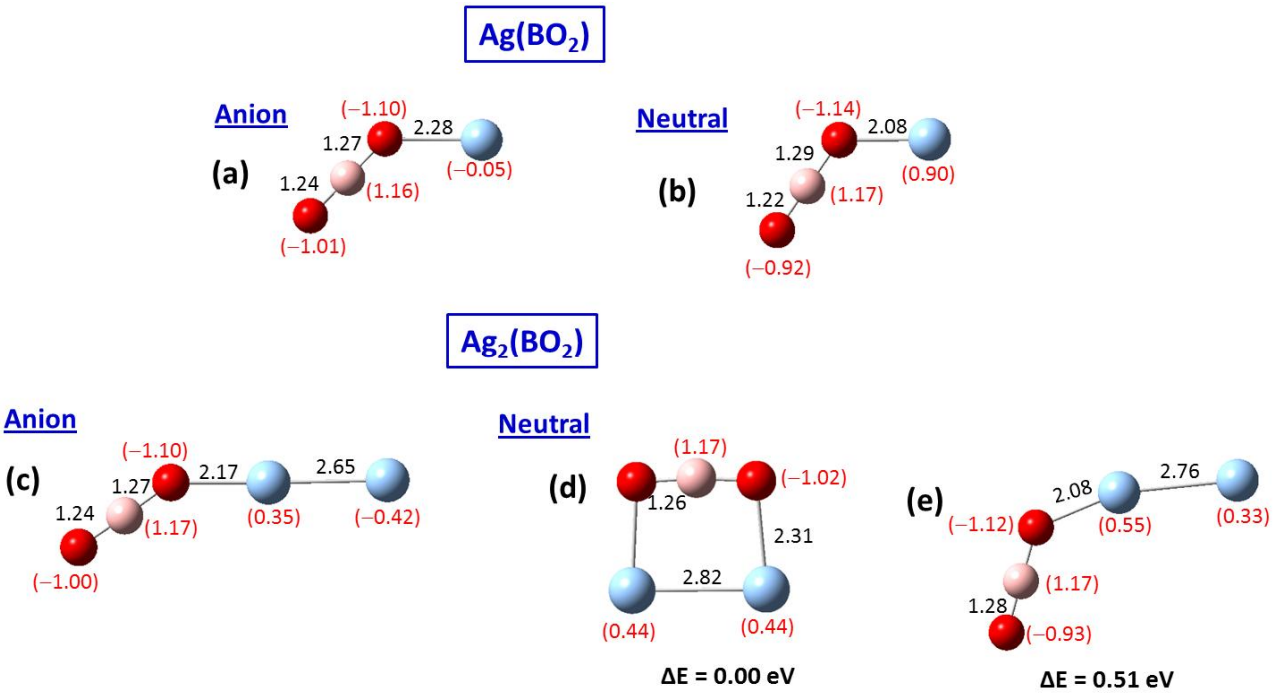

Figure 3. The ground state and higher energy isomers of negatively charged and neutral $Ag_n(BO_2)$ (n=1-2) clusters calculated employing the ωB97XD method. The relative energies to the most stable isomers are shown under the geometry structures. NPA charges of each atom were also displayed in the parentheses. All the bond lengths are given in Å.

The ground state geometry of the $[Ag_2(BO_2)]^-$ cluster is a bent-structure (Figure 3(c)), in which the BO_2 moiety is bound to a single Ag atom of the Ag_2 unit. This bent structure is similar to the previously reported ground state structures of the other corresponding coinage-metal borate clusters, namely $[Cu_2(BO_2)]^-$ [Ref. 29] and $[Au_2(BO_2)]^-$ [Ref. 27] clusters. On the other hand, the neutral $Ag_2(BO_2)$ cluster prefers to form a closed rhombus shaped structure (Fig. 3 (d)), whereas the open bent structure, the ground state geometry of anionic cluster, is found to be 0.51 eV higher in energy

(Fig. 3(e)). The ground state structure of the neutral $Ag_2(BO_2)$ cluster (Fig. 3(d)), surprisingly, is not a minimum on the potential energy surface of the anionic $Ag_2(BO_2)$ cluster and the geometry optimization of the closed rhombus-like structure resulted in the open bent structure. The structural change from a closed-rhombus shape to an open-bent shape is a consequence of accommodating the extra electron's charge on the $Ag_2(BO_2)$ cluster. Interestingly, the ground state geometries of neutral $Ag_2(BO_2)$ and the previously reported[27] $Au_2(BO_2)$ clusters are not similar; however their anionic counterparts do have similar geometries. The calculated VDE value of $[Ag_2(BO_2)]^-$ cluster is 3.71 eV. This value is in good agreement with the measured VDE values of 3.77 eV. Our simulated DOS spectrum (given in Figure 6) of the anionic ground state structure (open bent structure) can rebuild the experimental photoelectron spectrum of $[Ag_2(BO_2)]^-$ cluster, thereby indicating that the open bent structure is observed in the cluster beam. The first peak in the photoelectron spectrum of $[Ag_2(BO_2)]^-$ corresponds to ejection of electron from the HOMO, while the second peak is due to the ejection of electron from the (HOMO – 1) molecular orbital. Since the ground state geometries of neutral and anionic $Ag_2(BO_2)$ cluster are completely different, the calculated EA value of 3.09 eV is significantly lower than the measured ADE value of 3.59 eV. On the other hand, the energy difference between the ground state anion (Fig. 3(c)) and structurally similar neutral cluster (Fig. 3(e)), which corresponds to calculated ADE value, is 3.60 eV. This calculated ADE value is in good agreement with the measured ADE value of 3.59 eV, confirming that the measured ADE value of the anionic cluster does not correspond to the EA value of its neutral counterpart.

The NPA charge analysis carried out on the neutral and anionic $Ag_n(BO_2)$ (n = 1, 2) clusters not only reveal the nature of bonding between the Ag_n and BO_2 moieties, but also helps us to understand the trends in the VDE and ADE values of all the coinage-metal borate clusters as we move down from Cu to Au, This is achieved by comparing the charge distributions in $Ag_n(BO_2)$ (n = 1, 2) clusters with those previously reported for $Cu_n(BO_2)$[29] and $Au_n(BO_2)$[27] clusters. First, we start with the NPA charge distribution in neutral and anionic $Ag(BO_2)$ cluster which can be viewed from two

different perspectives, depending on how these clusters form. $[Ag(BO_2)]^-$ could be born as an anion or by attaching an electron to its born-neutral species. Note that the neutral $Ag(BO_2)$ cluster can be considered as a supersalt composed Ag and BO_2 superhalogen since a charge of $-0.90e$ is transferred from Ag atom to the BO_2 moiety. When the extra electron is added to the neutral cluster, 95% of this extra-electron's charge goes to the positively charged Ag atom. As a result, we observe that the charge on BO_2 moiety remains the same as one goes from neutral to anion, while the Ag atom regains its original electronic configuration with the aid of the extra electron. On the other hand, if the $[Ag(BO_2)]^-$ cluster was born as an anion, the added electron will reside on the BO_2 moiety as it mimics a halogen atom. During the anion photoelectron spectroscopy, the electron will likely photo-detach from the silver atom as it can then form a closed electronic shell, thus, leaving it in a positively charged metal-center in the resulting neutral cluster. A similar scenario of a significant charge transfer ($-0.87e$) was reported[29] earlier in the neutral $Cu(BO_2)$ cluster, while in the case of neutral $Au(BO_2)$ cluster only 68% of electron charge transfer was reported.[27] Based on these charge distributions, the bonding in $Cu(BO_2)$ and $Ag(BO_2)$ clusters is termed ionic, while in the case of $Au(BO_2)$ cluster, it is partially covalent. Since, in both $[Cu(BO_2)]^-$ and $[Ag(BO_2)]^-$ clusters, the photodetached electron is coming from the metal atom, the calculated VDE values of these clusters are similar to each other (2.17 eV and 2.32 eV, respectively). On the other hand, in the case of $[Au(BO_2)]^-$ cluster, it was reported[27] that the extra-electron was distributed over the entire cluster, and the photodetachment of the delocalized-electron charge resulted in a higher VDE value of 3.34 eV.

We now turn to the charge distribution in neutral and anionic $Ag_2(BO_2)$ cluster. In both the isomers of neutral $Ag_2(BO_2)$ cluster, the BO_2 moiety gains a charge of $-0.88e$ from the Ag_2 unit. In the ground state structure (Fig. 3(d)), each Ag atom loses $-0.44e$ of charge, while in the case of the higher energy bent isomer (Fig. 3(e)), the terminal Ag atom has a charge of $+0.33e$ and the Ag atom bonded to the BO_2 unit has a charge of $+0.55e$. Thus, in $Ag_2(BO_2)$ cluster the interaction between

BO_2 and Ag_2 units is primarily ionic in nature. Comparison of the charge distribution in the anionic (Fig 3(c)) and its corresponding neutral isomer (Fig. 3(e)) reveals that during the photodetachment process, 75% of the electron's charge comes from the terminal Ag atom, while 20% of the electron's charge comes from the Ag atom that is bound to the BO_2 unit. Thus, the Ag_2 unit loses 95% of the charge in the photodetachment process. Again, a similar scenario was observed in $Cu_2(BO_2)$ cluster[29] as well, where the Cu_2 unit loses 87% of the charge during the photodetachment. However, this is in contrast to the charge distribution reported[27] for $Au_2(BO_2)$ cluster, where Au_2 loses only 75% of its charge, while the rest comes from the BO_2 unit. Therefore, compared to the VDE/ADE values of $[Cu_2(BO_2)]^-$ (3.68/3.44 eV) and $[Ag_2(BO_2)]^-$ (3.71/3.60 eV), the VDE and ADE values of $Au_2(BO_2)$ are significantly larger at 4.80 eV and 4.66 eV, respectively. It seems the trends in VDE and ADE values of $M_n(BO_2)$ (M = coinage-metal; n = 1-2) clusters are consistent with their corresponding NPA charge distributions. Thus, the NPA charge distributions in the neutral and anionic $M_n(BO_2)$ (M = Cu, Ag, and Au; n = 1, 2) clusters help us understand the nature of bonding and variations in the VDE and ADE values of these clusters as we go from Cu to Ag, and to Au.

B. $Ag_n(BO_2)_2$ (n = 1 – 3) clusters:

The lowest energy and relevant higher energy isomers of neutral and anionic $Ag(BO_2)_2$ and $Ag_2(BO_2)_2$ clusters are shown in Figure 4, while those of $Ag_3(BO_2)_2$ cluster are given in Figure 5. The ground state geometry of $[Ag(BO_2)_2]^-$ cluster has a *trans* configuration (Fig. 4(a)) in which the BO_2 moieties are bonded separately on to either sides of the Ag atom. Interestingly, the lowest energy isomer of neutral $Ag(BO_2)_2$, is completely different from its anionic counterpart. The ground state structure of neutral $Ag(BO_2)_2$ can be viewed as an Ag atom bonded to a B_2O_4 unit (see Fig. 4(b)), while the *trans* configuration (Fig. 4(c)) is found to be 1.19 eV higher in energy. Our calculated VDE and ADE values of $[Ag(BO_2)_2]^-$ are 6.25 and 6.16 eV, respectively. These values are in good agreement with the experimental VDE and ADE values of 6.28 and 6.20 eV, respectively.

The simulated DOS spectrum of the ground state $[Ag(BO_2)_2]^-$, shown in Figure 6, agrees well with the reported photoelectron spectrum indicating that it is the *trans* configuration of $[Ag(BO_2)_2]^-$ that is produced in the cluster beam. The VDE/ADE values of $[Ag(BO_2)_2]^-$ are unusually high compared to those of the corresponding coinage-metal borate clusters, namely $[Cu(BO_2)_2]^-$ (5.28/5.07 eV) and $[Au(BO_2)_2]^-$ (5.9/5.7 eV).[28, 29] This unusual result, namely the VDE/ADE values of $Ag(BO_2)_2$ being higher than those of $Au(BO_2)_2$, was reported due to significant spin-orbit coupling (SOC) effects in $Au(BO_2)_2$ clusters.[34] Based on these significantly large VDE and ADE values, $Ag(BO_2)_2$ is also a hyperhalogen, similar to $Cu(BO_2)_2$ and $Au(BO_2)_2$ clusters. A comparison of the NPA charge distribution in the anionic ground state structure (Fig. 4(a)) and its structurally identical neutral isomer (Fig. 4(c)) reveals that the extra-electron is delocalized over the entire cluster, with 34% of the charge on the Ag atom, and the remaining 66% distributed uniformly over the two BO_2 moieties. Unlike in the above discussed cases of $[Ag(BO_2)]^-$ and $[Ag_2(BO_2)]^-$ where the extra electron is localized over the metal atom/s, in $Ag(BO_2)_2$ cluster the extra electron is delocalized over the entire cluster, thus resulting in an unusually large VDE and ADE values.

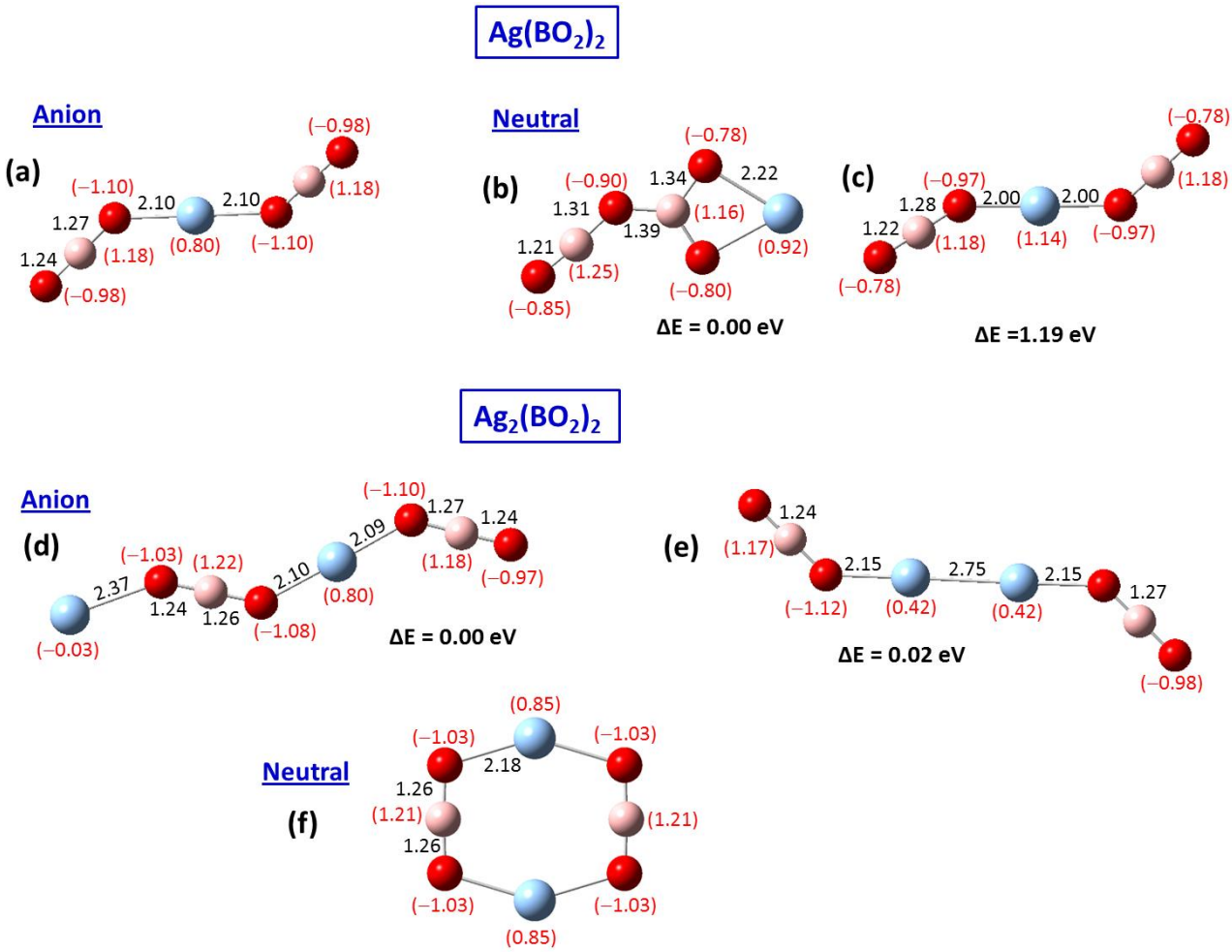

Figure 4. The ground state and higher energy isomers of negatively charged and neutral $Ag_n(BO_2)_2$ (n=1-2) clusters calculated employing the ωB97XD method. The relative energies to the most stable isomers are shown under the geometry structures. NPA charges of each atom were also displayed in the parentheses. All the bond lengths are given in Å.

For $[Ag_2(BO_2)_2]^-$ cluster, our calculations reveal two energetically degenerate (ΔE = 0.02 eV) chain-like structures (Fig. 4(d) and Fig. 4(e)) to be lowest in energy. These isomers can be visualized as bonding of two units of $Ag(BO_2)$ clusters in two different ways: The first isomer (Fig. 4(d)) can be built by combining two Ag-OBO units with the Ag atom of one of the $Ag(BO_2)$ units acting as a bridge between these units, thereby resulting in ($Ag\text{-}BO_2\text{-}Ag\text{-}BO_2$) structure. This isomer can also be obtained by adding a Ag atom to one end of the $[Ag(BO_2)_2]^-$ cluster. The second isomer (Fig. 4(e)) can be described as two BO_2 units bound together by a Ag-Ag bridge to form an ($BO_2\text{-}AgAg\text{-}BO_2$) structure. The calculated VDE value of the first isomer, $Ag\text{-}BO_2\text{-}Ag\text{-}BO_2$, is 3.37 eV, which agrees

well with the experimental VDE of 3.32 eV. Interestingly, the VDE of the second isomer, BO_2-Ag_2-BO_2, is calculated to be 5.49 eV, which fits well with the second feature (~5.64 eV) in the experimental photoelectron spectrum of $[Ag_2(BO_2)_2]^-$ cluster. So we simulated the DOS to find out whether the second isomer, (BO_2-Ag_2-BO_2), contributes to the experimental spectrum. As we can see in Figure 6, both isomers together rebuild the experimental photoelectron spectrum of $[Ag_2(BO_2)_2]^-$ cluster. So, we conclude that both isomers, (Ag-BO_2-Ag-BO_2) and (BO_2-Ag_2-BO_2) coexist in the experiment. Considering the high VDE value of BO_2-Ag_2-BO_2 isomer, it can be classified as a hyperhalogen.

The neutral $Ag_2(BO_2)_2$ cluster, interestingly, prefers to form a ring-like structure [Fig. 4(f)]. The two chain-like lowest energy isomers of the anion assumed the ring structure after geometry optimization. The chain-like Ag-BO_2-Ag-BO_2 structure (not shown in Figure 4) was stabilized at a higher spin-triplet state. This chain structure was found to be 1.46 eV higher in energy than the ring structure. It is noteworthy here that the lowest energy isomers of neutral and anionic $Ag_2(BO_2)_2$ cluster are identical to the corresponding $Cu_2(BO_2)_2$ cluster reported earlier.[29] However, unlike in the current situation, only one isomer, namely Cu-BO_2-Cu-BO_2 was reported[29] to be contributing towards the photoelectron spectrum of $[Cu_2(BO_2)_2]^-$ cluster.

The NPA charge analysis of both the anionic isomers, Ag-BO_2-Ag-BO_2 and BO_2-Ag_2-BO_2, together with the neutral ground state structure of $Ag_2(BO_2)_2$ cluster reveals an interesting picture. In the case of the Ag-BO_2-Ag-BO_2 isomer, the bridging Ag atom loses a charge of –0.80*e* to the BO_2 units, while the terminal Ag atom gains a small negative charge of –0.03*e*. On the other hand, in BO_2-Ag_2-BO_2 isomer, each of the bridging Ag atoms lose same amount of charge (–0.42*e*) to the BO_2 units. On comparing these charge distributions with the charges on neutral $Ag_2(BO_2)_2$ cluster, it can be concluded that in the case of BO_2-Ag_2-BO_2 isomer, the extra-electron is delocalized, with a majority (86%) of the extra-electron's charge going to the Ag atoms. This delocalization of the extra-electron in BO_2-Ag_2-BO_2 isomer results in an unusually large VDE value of 5.49 eV and is

classified as a hyperhalogen. On the other hand, a comparison of charges on anionic Ag-BO_2-Ag-BO_2 isomer and the neutral ground state structure shows that the terminal Ag atom in Ag-BO_2-Ag-BO_2 isomer loses 88% of the charge during the photo-ejection of the extra-electron. Thus, the photodetachment of localized electron results in a comparatively lower VDE of 3.37 eV.

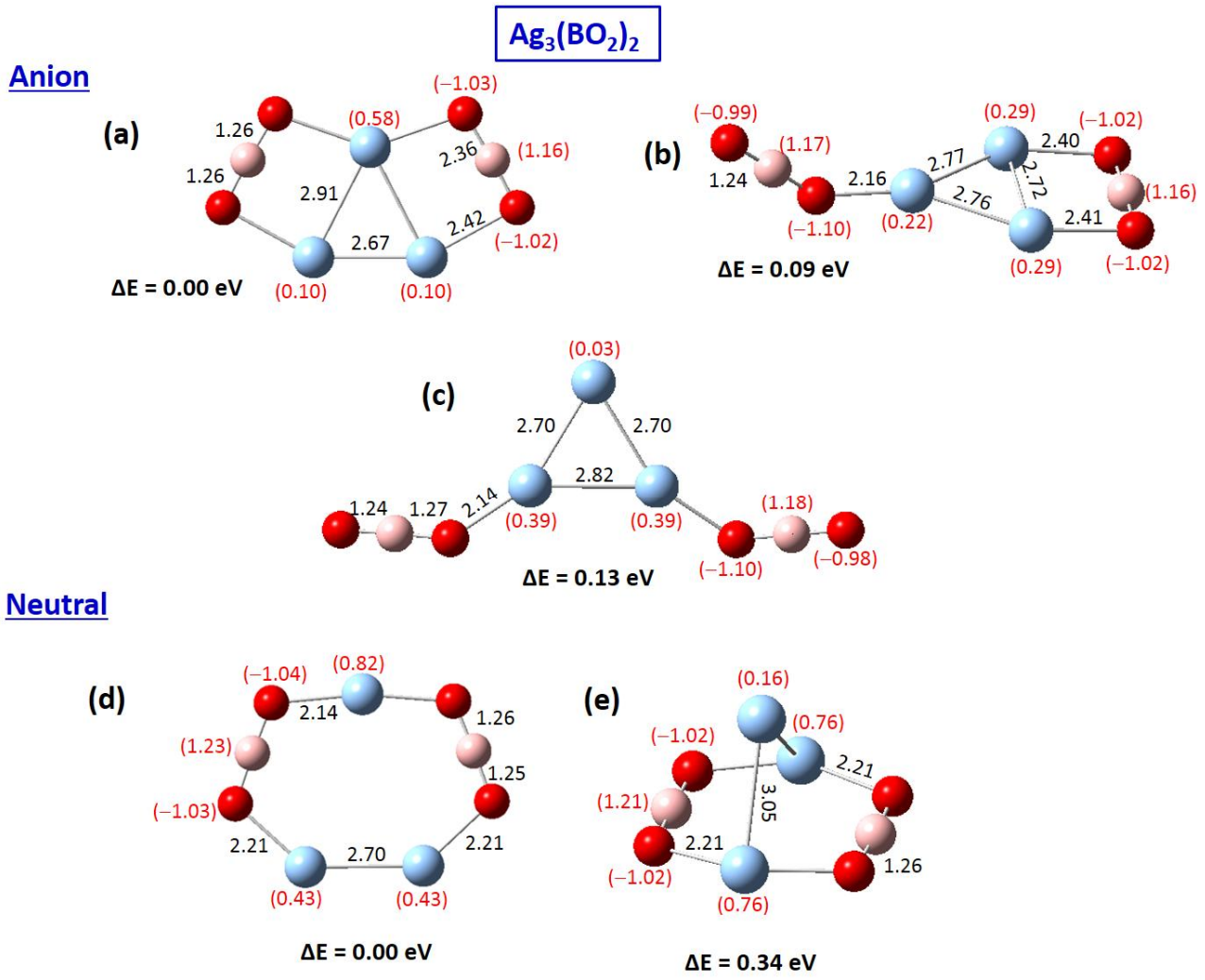

Figure 5. The ground state and higher energy isomers of negatively charged and neutral $Ag_3(BO_2)_2$ cluster calculated employing the ωB97XD method. The relative energies to the most stable isomers are shown under the geometry structures. NPA charges of each atom were also displayed in the parentheses. All the bond lengths are given in Å.

We now turn to the largest cluster under the current study, namely, $Ag_3(BO_2)_2$ cluster. In the case of $[Ag_3(BO_2)_2]^-$ cluster, our calculations reveal three low-lying isomers (ΔE_{max} = 0.13 eV) with a general form of BO_2–Ag_3–BO_2 structure (see Fig. 5). These three isomers differ in the way the two

BO_2 superhalogen units are bound to the Ag_3 triangular moiety. In the lowest energy isomer [Fig. 5(a)], the two BO_2 units are bound to the two opposite edges of the Ag_3 triangular moiety forming a planar structure with four Ag – O bonds. On the other hand, in the second isomer [Fig. 5(b)], which is iso-energetic with the lowest energy structure ($\Delta E = 0.09$ eV), only one of the BO_2 units is bound to the edge of the Ag_3 triangle, while the other BO_2 unit is bound to the corner (i.e., Ag atom) of the Ag_3 triangle, thereby resulting in a non-planar structure with three Ag – O bonds. In the third isomer [Fig. 5(c)], which is 0.13 eV higher in energy, both BO_2 units are bonded separately to two corners (i.e., Ag atoms) of the Ag_3 triangular moiety. The VDE values of the first isomer [Fig 5(a)] and the second isomer [Fig. 5 (b)] are calculated to be 4.01 and 4.91 eV, respectively. While the VDE value of the first isomer is in agreement with the measured value of 4.17 eV, the VDE value of the second isomer matches very well with the second peak of the $[Ag_3(BO_2)_2]^-$ photoelectron spectrum, observed at 4.98 eV. Interestingly, the calculated VDE of the third isomer [Fig. 5(c)] is 5.89 eV, which matches well with the feature around 5.9 eV in the experimental spectrum. A comparison of the DOS simulation of the three isomers with the experimental photoelectron spectrum, as shown in Figure 6, indicates the presence of the first two isomers in the cluster beam, while the presence of the third isomer cannot be ruled out as its DOS spectrum matches the high EBE peak very well and its energy is only slightly higher than the second isomer. Since, the VDE of the second and third isomers of $[Ag_3(BO_2)_2]^-$ cluster are greater than that of the BO_2 superhalogen building block, we can classify the corresponding neutral cluster of these isomers as hyperhalogens.

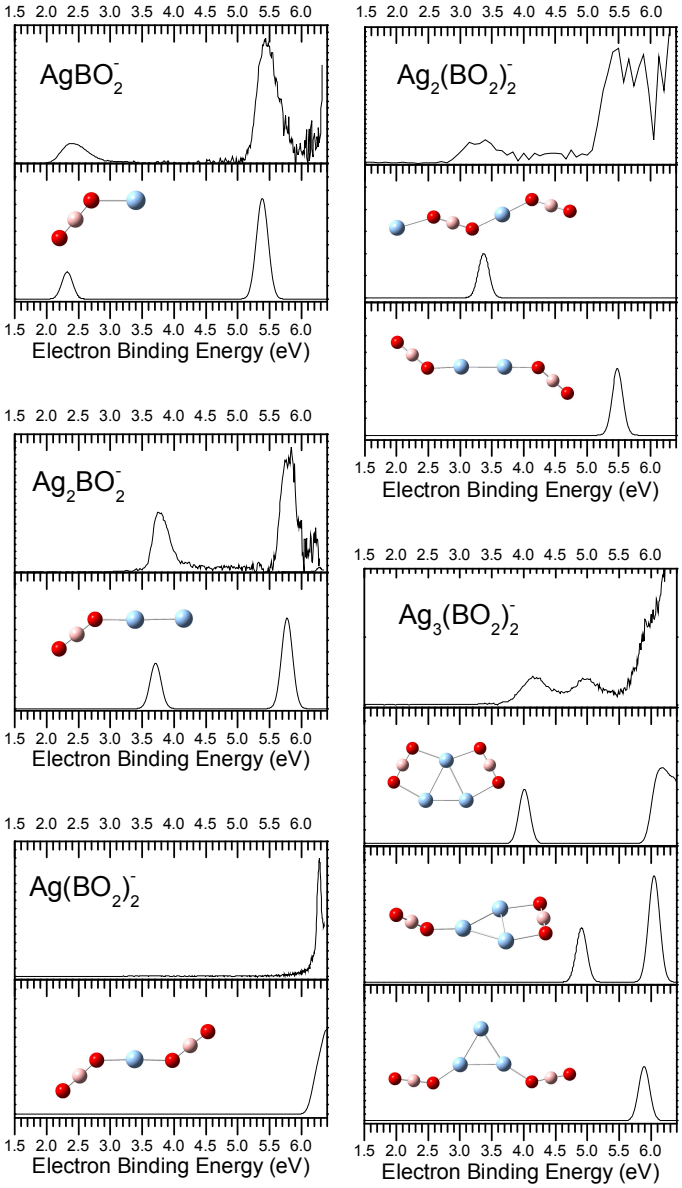

Figure 6. Comparison of the experimental photoelectron spectra of $[Ag_n(BO_2)_m]^-$ (n=1-3, m=1-2) clusters with their simulated DOS spectra. The simulations were conducted by fitting the distribution of the transition lines with unit-area Gaussian functions of 0.2 eV full widths at half maximum (FWHM).

The most stable structure of neutral $Ag_3(BO_2)_2$ cluster is a planar ring structure [Fig. 5 (d)], similar to that of the lowest energy isomer of $[Ag_3(BO_2)_2]^-$ cluster, but without any bonds between the Ag atoms. Interestingly, neither of the two low-lying isomers of anion are found to be a minimum on the potential energy surface of the neutral cluster. After geometry optimization, these two isomers

resulted in the same planar ring structure. Our calculations show that the ionization potential (IP) of Ag_3 is 5.8 eV, which is comparable to the ionization potential (IP) value of lithium (5.4 eV). Therefore, the Ag_3 moiety can be considered as a pseudo-alkali (PA). So, one can view the $Ag_3(BO_2)_2$ cluster as a combination of a pseudo-alkali Ag_3 moiety and two BO_2 superhalogen (SH) units: (SH – PA – SH). Since, a pseudo-alkali can donate an electron easily; we expect a strong ionic interaction between the Ag_3 moiety and the BO_2 unit. The NPA charge analysis of the neutral $Ag_3(BO_2)_2$ cluster shows that this is indeed the case. In the neutral $Ag_3(BO_2)_2$, there is a charge transfer of almost two electrons from the Ag_3 moiety to the two BO_2 superhalogen units, with a charge of +1.68*e* on Ag_3 and a charge of –0.84*e* on each of the BO_2 units. However, being a pseudo-alkali, Ag_3 moiety prefers to lose only one electron, but not almost two, as observed in the neutral $Ag_3(BO_2)_2$ cluster. Thus, one can say that in the neutral $Ag_3(BO_2)_2$ cluster, the Ag_3 moiety is short of one electron to be stabilized. Therefore, when an extra-electron is added to the $Ag_3(BO_2)_2$ cluster, majority of this electron's charge (90%) went to the Ag_3 moiety, thereby resulting in a +1*e* charge on it, while the rest of 10% was equally distributed over two BO_2 superhalogen units. This delocalization of the extra-electron's charge resulted in a large VDE/ADE values for $[Ag_3(BO_2)_2]^-$ cluster. If one tries to understand this charge distribution from the experimental view point, one can then say that during the photodetachment, the electron is removed from the positively charged Ag_3 moiety, thereby creating an almost doubly-charged Ag_3 in the resulting neutral cluster.

IV. Summary

In summary, we have carried out a systematic study of neutral and anionic $Ag_n(BO_2)_m$ (n = 1 – 3, m = 1 – 2) clusters using anion photoelectron spectroscopy and density functional theory based calculations. The ground state structures of neutral $Ag_2(BO_2)$ and $Ag_n(BO_2)_2$ (*n*=1-3) clusters are very different from their anionic counterparts. While the neutral clusters prefer to form closed-ring like structures, their corresponding anionic clusters form more open chain-like structures. In addition,

a comparison between our calculated results and the photoelectron spectra of $[Ag_2(BO_2)_2]^-$ and $[Ag_3(BO_2)_2]^-$ clusters revealed the presence of multiple isomers in the cluster beam. Among these multiple-isomers, the higher energy isomers were found to have a significantly larger VDE than the lower energy isomers, thereby contributing towards the higher energy peaks in the photoelectron spectra. Among all the clusters under the current study, $Ag(BO_2)_2$ and the neutral counterparts of higher energy isomers of $[Ag_2(BO_2)_2]^-$ and $[Ag_3(BO_2)_2]^-$ clusters are found to be hyperhalogens.

ACKNOWLEDGEMENTS

This work was supported by the Knowledge Innovation Program of the Chinese Academy of Sciences (Grant No. KJCX2-EW-H01) and the Natural Science Foundation of China (Grant No. 21103202). A portion of theoretical calculations were conducted on the ScGrid and DeepComp 7000 of the Supercomputing Center, Computer Network Information Center of the Chinese Academy of Sciences. A. K. K. acknowledges the support of WCU College of Arts and Science (CAS) in providing the start-up funds. P.J. acknowledges partial support from the U.S. Department of Energy, Office of Basic Energy Sciences, Division of Materials Sciences and Engineering under Award # DE-FG02-96ER45579.

REFERENCES

1. N. Bartlett, *Proc. Chem. Soc.*,1962, 218.
2. N. Bartlett and D. H. Lohmann, *Proc. Chem. Soc.*, 1962, 115-116.
3. U. Berzinsh, M. Gustafsson, D. Hanstorp, A. Klinkmüller, U. Ljungblad, and A. M. Mårtensson-Pendrill, *Phys. Rev. A*, 1995, **51**, 231-238.
4. G. L. Gutsev and A. I. Boldyrev, *Chem. Phys.*, 1981, **56**, 277-283.

5. G. L. Gutsev and A. I. Boldyrev, *J. Phys. Chem.*, 1990, **94**, 2256-2259.

6. A. I. Boldyrev and W. von Niessen, *Chem. Phys.*, 1991, **155**, 71-78.

7. A. I. Boldyrev and J. Simons, *J. Chem. Phys.*, 1992, **97**, 2826-2827.

8. A. I. Boldyrev and J. Simons, *J. Chem. Phys.*, 1993, **99**, 4628-4637.

9. G. L. Gutsev, P. Jena, and R. J. Bartlett, *Chem. Phys. Lett.*, 1998, **292**, 289-294.

10. G. L. Gutsev, B. K. Rao, P. Jena, X.-B. Wang, and L.-S. Wang, *Chem. Phys. Lett.*, 1999, **312**, 598-605.

11. X.-B. Wang, C.-F. Ding, L.-S. Wang, A. I. Boldyrev, and J. Simons, *J. Chem. Phys.*, 1999, **110**, 4763-4771.

12. G. L. Gutsev, P. Jena, H.-J. Zhai, and L.-S. Wang, *J. Chem. Phys.*, 2001, **115**, 7935-7944.

13. I. Anusiewicz and P. Skurski, *Chem. Phys. Lett.*, 2002, **358**, 426-434.

14. I. Anusiewicz, M. Sobczyk, I. Dąbkowska, and P. Skurski, *Chem. Phys.*, 2003, **291**, 171-180.

15. X. Yang, X.-B. Wang, L.-S. Wang, S. Niu, and T. Ichiye, *J. Chem. Phys.*, 2003, **119**, 8311-8320.

16. M. Sobczyk, A. Sawicka, and P. Skurski, *Eur. J. Inorg. Chem.*, 2003, **2003**, 3790-3797.

17. A. N. Alexandrova, A. I. Boldyrev, Y.-J. Fu, X. Yang, X.-B. Wang, and L.-S. Wang, *J. Chem. Phys.*, 2004, **121**, 5709-5719.

18. B. M. Elliott, E. Koyle, A. I. Boldyrev, X.-B. Wang, and L.-S. Wang, *J. Phys. Chem. A*, 2005, **109**, 11560-11567.

19. I. Anusiewicz and P. Skurski, *Chem. Phys. Lett.*, 2007, **440**, 41-44.

20. I. Anusiewicz, *Aust. J. Chem.*, 2008, **61**, 712-717.

21. J. Yang, X.-B. Wang, X.-P. Xing, and L.-S. Wang, *J. Chem. Phys.*, 2008, **128**, 201102.

22. P. Koirala, M. Willis, B. Kiran, A. K. Kandalam, and P. Jena, *J. Phys. Chem. C*, 2010, **114**, 16018-16024.

23. K. Pradhan, G. L. Gutsev, and P. Jena, *J. Chem. Phys.*, 2010, **133**, 144301.

24. M. M. Wu, H. Wang, Y. J. Ko, Q. Wang, Q. Sun, B. Kiran, A. K. Kandalam, K. H. Bowen, and P. Jena, *Angew. Chem. Int. Ed.*, 2011, **50**, 2568-2572.

25. K. Pradhan, G. L. Gutsev, C. A. Weatherford, and P. Jena, *J. Chem. Phys.*, 2011, **134**, 234311.

26. Y. J. Ko, H. Wang, K. Pradhan, P. Koirala, A. K. Kandalam, K. H. Bowen, and P. Jena, *J. Chem. Phys.*, 2011, **135**, 244312.

27. M. Götz, M. Willis, A. K. Kandalam, G. F. Ganteför, and P. Jena, *ChemPhysChem*, 2010, **11**, 853-858.

28. M. Willis, M. Götz, A. K. Kandalam, G. F. Ganteför, and P. Jena, *Angew. Chem. Int. Ed.*, 2010, **49**, 8966-8970.

29. Y. Feng, H.-G. Xu, W. J. Zheng, H. Zhao, A. K. Kandalam, and P. Jena, *J. Chem. Phys.*, 2011, **134**, 094309.

30. K. Pradhan and P. Jena, *J. Chem. Phys.*, 2011, **135**, 144305.

31. G. L. Gutsev, C. A. Weatherford, L. E. Johnson and P. Jena, *J. Comput. Chem.*2012, **33**, 416-424.

32. C. Paduani and P. Jena, *J. Phys. Chem. A*, 2012, **116**, 1469-1474.

33. P. Koirala, K. Pradhan, A. K. Kandalam and P. Jena, *J. Phys. Chem. A*, 2013, **117**, 1310-1318.

34. H. Chen, X. Y. Kong, W. J. Zheng, J. N. Yao, A. K. Kandalam and P. Jena, *ChemPhysChem*, 2013, **14**, 3303-3308.

35. H.-G. Xu, Z.-G. Zhang, Y. Feng, J. Y. Yuan, Y. C. Zhao and W. J. Zheng, *Chem. Phys. Lett.*, 2010, **487**, 204-208.

36. J.-D. Chai and M. Head-Gordon, *Phys. Chem. Chem. Phys.*, 2008, **10**, 6615-6620.

37. M. J. Frisch, G. W. Trucks, H. B. Schlegel and e. al., Gaussian 09, Revision C. 01, Gaussian, Inc., Wallingford CT, 2010.

38. C. Lee, W. Yang and R. G. Parr, *Phys. Rev. B*, 1998, **37**, 785-789.

39. A. Becke, *J. Chem. Phys.*, 1993, **98**, 5648-5652.

40. Y. Zhao and D. Truhlar, *Theor. Chem. Acc.*, 2008, **120**, 215-241.

41. J. T. David and C. H. Nicholas, *J. Chem. Phys.*, 1998, **109**, 10180-10189.

42. J. Akola, M. Manninen, H. Hakkinen, U. Landman, X. Li and L.-S. Wang, *Phys. Rev. B*, 1999, **60**, R11297-R11300.

43. X. Y. Kong, H.-G. Xu and W. J. Zheng, *J. Chem. Phys.*, 2012, **137**, 064307.